International Journal of
Molecular Sciences

MDPI

Article

DFT Study of Molecular Structure, Electronic and Vibrational Spectra of Tetrapyrazinoporphyrazine, Its Perchlorinated Derivative and Their Al, Ga and In Complexes

Igor V. Ryzhov, Alexey V. Eroshin, Yuriy A. Zhabanov *, Daniil N. Finogenov and Pavel A. Stuzhin

Research Institute of Chemistry of Macroheterocyclic Compounds, Ivanovo State University of Chemistry and Technology, Sheremetievskiy Av. 7, 153000 Ivanovo, Russia; ryzhoff.ihor@yandex.ru (I.V.R.); alexey.yeroshin@gmail.com (A.V.E.); dan.finogenof@gmail.com (D.N.F.); stuzhin@isuct.ru (P.A.S.)
* Correspondence: zhabanov@isuct.ru; Tel.: +7-4932-35-98-74

Abstract: Electronic and geometric structures of metal-free, Al, Ga and In complexes with tetrapyrazinoporphyrazine (TPyzPA) and octachlorotetrapyrazinoporphyrazine ($TPyzPACl_8$) were investigated by density functional theory (DFT) calculations and compared in order to study the effect of chlorination on the structure and properties of these macrocycles. The nature of the bonds between metal atoms and nitrogen atoms was described using the NBO-analysis. Simulation and interpretation of electronic spectra were performed with the use of time-dependent density functional theory (TDDFT). A description of calculated IR spectra was carried out based on the analysis of the distribution of the potential energy of normal vibrational coordinates.

Keywords: tetrapyrazinoporphyrazine; octachlorotetrapyrazinoporphyrazine; DFT study; molecular and electronic structure; electronic spectra; vibrational spectra

check for updates

Citation: Ryzhov, I.V.; Eroshin, A.V.; Zhabanov, Y.A.; Finogenov, D.N.; Stuzhin, P.A. DFT Study of Molecular Structure, Electronic and Vibrational Spectra of Tetrapyrazinoporphyrazine, Its Perchlorinated Derivative and Their Al, Ga and In Complexes. *Int. J. Mol. Sci.* **2022**, *23*, 5379. https://doi.org/10.3390/ijms23105379

Academic Editor: Henry Chermette

Received: 18 April 2022
Accepted: 9 May 2022
Published: 11 May 2022

1. Introduction

Tetrapyrrole macroheterocycles are essential for a wide range of technologies, including optoelectronics and information storage devices [1–7]. The complexes of tetrapyrazinoporphyrazine ($H_2TPyzPA$) with metals possessing π-deficient heterocyclic fragments are promising compounds for organic electronics [8–11]. The results of the recent electrochemical study [8] of the perchlorinated complexes $M(Cl)TPyzPACl_8$ (M = Al, Ga, In) allow them to be considered as potential acceptor materials. Recently this was also demonstrated for perchlorinated tripyrazinosubporphyrazines [12].

Fine tuning of the physico-chemical properties of the metal complexes with macroheterocyclic ligands requires a deep knowledge of their molecular and electronic structures. However, only a little attention has, of yet, been paid to structural investigations of the metal complexes of TPyzPA [13]. Solid-state X-ray studies of Fe(II) [14] and Sn(IV) complexes [15] revealed that the $TPyzPACl_8$ macrocycle is nearly planar. The possible planarity of the structures of $MTPyzPACl_8$ complexes gives rise to the extended π-electron conjugation, which in turn results in an increased packing density.

The present contribution is devoted to the combined computational investigation of the geometry structures, features of the metal–ligand bonding and spectral properties of M(Cl)TPyzPA (M = Al, Ga, In) complexes and their perchlorinated analogues. It also extends our recent study [16] of the tetrabenzoporphyrin (TBP) complexes with the same set of metals. Density functional theory (DFT) [17,18] was used as a theoretical framework since it was earlier established to provide a good description of the features of the geometry and electronic structures of the analogous macroheterocycles and their metal complexes [16,19–25].

2. Results

2.1. Molecular Structures

According to the performed quantum chemical calculations, the equilibrium structures of the Al(III), Ga(III) and In(III) complexes of tetrapyrazinoporphyrazine (M(Cl)TPyzPA) and their perchlorinated analogues are doming-distorted and possess C_{4v} symmetry (Figure 1). The distortion is caused by a metal atom as the metal-free H_2TPyzPA and H_2TPyzPACl_8 molecules are planar (D_{2h} symmetry). The H_2TPyzPA internuclear distances obtained by the authors of [26] are systematically higher compared to our data. This discrepancy can be explained by the use of corrections for the dispersion interaction in this paper and pseudopotentials in [26]. The H_2TPyzPA bond lengths calculated in [27] are also systematically higher than those obtained in this work. The main geometric parameters of compounds under consideration are given in Table 1.

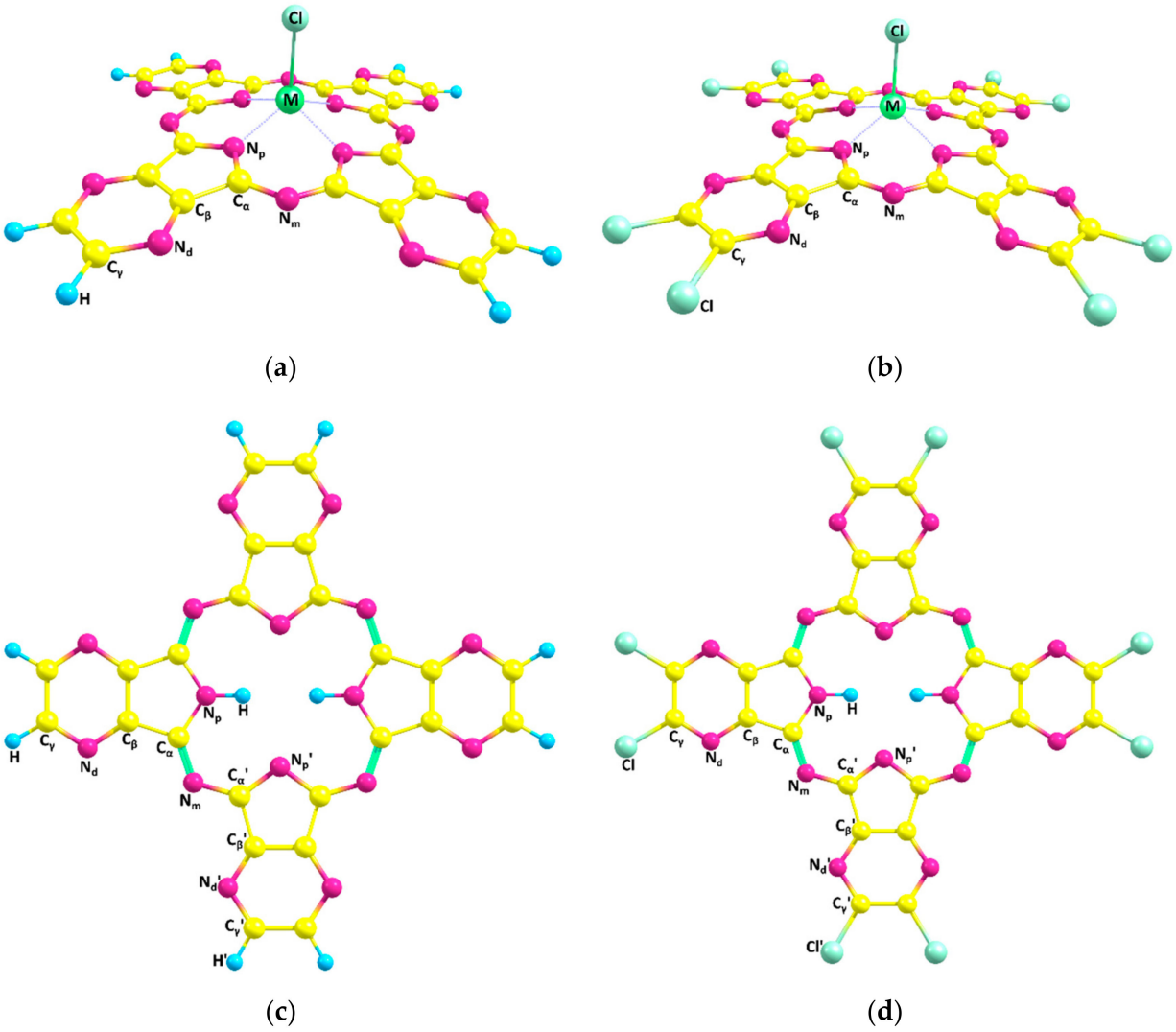

Figure 1. Molecular structures of the Al(III), Ga(III) and In(III) complexes with pyrazinoporphyrazine (M(Cl)TPyzPA) (**a**), octachloropyrazinoporphyrazines (M(Cl)TPyzPACl_8) (**b**) and metal-free molecules ((**c**) and (**d**), respectively) with atom labeling.

Table 1. Internuclear distances (r_e, in Å) and valence angles (∠, in deg.) of the equilibrium structures by PBE0-D3/def2-TZVP calculations.

	Al(Cl)TPyzPA	**Ga(Cl)TPyzPA**	**In(Cl)TPyzPA**	**H_2TPyzPA**
Symmetry	C_{4v}	C_{4v}	C_{4v}	D_{2h}
		Distances		
M-N_p/M-N_p'	1.981	2.022	2.161	-
M-Cl_{ax}	2.145	2.187	2.336	-
N_p-C_α/N_p'-C_α'	1.371	1.367	1.364	1.368/1.355
C_α-N_m/C_α'-N_m	1.308	1.310	1.316	1.304/1.321
C_α-C_β/C_α'-C_β'	1.450	1.453	1.458	1.450/1.464
C_β-C_β/C_β'-C_β'	1.391	1.393	1.399	1.401/1.393
C_β-N_d/C_β'-N_d'	1.328	1.328	1.326	1.329/1.324
N_d-C_γ/N_d'-C_γ'	1.322	1.322	1.323	1.320/1.327
C_γ-C_γ/C_γ'-C_γ'	1.408	1.407	1.405	1.408/1.401
C_γ-H/C_γ'-H′	1.086	1.086	1.086	1.086/1.086
$(N_p \ldots N_p)_{opp}$	3.859	3.918	4.037	4.054/3.899
$(N_p \ldots N_p)_{adj}$	2.728	2.770	2.854	2.812
P [1]	21.432	21.416	21.440	21.376
		Bond angles		
∠($Cl_{ax}MN_p$)	103.1	104.3	110.9	-
∠(MN_pC_α)	125.2	124.5	123.6	123.2
∠($N_pC_\alpha N_m$)/($N_p'C_\alpha'N_m$)	127.9	128.0	128.0	128.5/128.1
∠($C_\alpha N_m C_\alpha'$)	122.5	123.4	125.5	124.2
∠($C_\alpha C_\beta N_d$)/($C_\alpha'C_\beta'N_d'$)	129.8	129.8	129.8	129.0/130.6
∠($C_\beta N_d C_\gamma$)/($C_\beta'N_d'C_\gamma'$)	113.2	113.3	113.6	113.6/113.3
M-X [2]	0.448	0.499	0.772	-
α [3]	175.5	174.3	164.7	180
	Al(Cl)TPyzPACl_8	**Ga(Cl)TPyzPACl_8**	**In(Cl)TPyzPACl_8**	**H_2TPyzPACl_8**
Symmetry	C_{4v}	C_{4v}	C_{4v}	D_{2h}
		Distances		
M-N_p/M-N_p'	1.980	2.021	2.162	-
M-Cl_{ax}	2.142	2.183	2.332	-
N_p-C_α/N_p'-C_α'	1.372	1.368	1.364	1.368/1.356
C_α-N_m/C_α'-N_m	1.308	1.310	1.316	1.304/1.321
C_α-C_β/C_α'-C_β'	1.447	1.450	1.455	1.448/1.461
C_β-C_β/C_β'-C_β'	1.384	1.387	1.392	1.394/1.386
C_β-N_d/C_β'-N_d'	1.330	1.329	1.328	1.330/1.325
N_d-C_γ/N_d'-C_γ'	1.305	1.306	1.307	1.304/1.310
C_γ-C_γ/C_γ'-C_γ'	1.433	1.432	1.430	1.433/1.424
C_γ-Cl/C_γ'-Cl′	1.709	1.709	1.709	1.709/1.712
$(N_p \ldots N_p)_{opp}$	3.856	3.915	4.031	4.051/3.892
$(N_p \ldots N_p)_{adj}$	2.726	2.768	2.850	2.809
P [1]	21.440	21.424	21.440	21.376
		Bond angles		
∠($Cl_{ax}MN_p$)	103.2	104.5	111.2	-
∠(MN_pC_α)	125.2	124.5	123.5	123.3
∠($N_pC_\alpha N_m$)/($N_p'C_\alpha'N_m$)	128.0	128.1	128.1	128.5/128.2
∠($C_\alpha N_m C_\alpha'$)	122.3	123.3	125.3	124.0
∠($C_\alpha C_\beta N_d$)/($C_\alpha'C_\beta'N_d'$)	130.3	130.3	130.3	129.5/131.1
∠($C_\beta N_d C_\gamma$)/($C_\beta'N_d'C_\gamma'$)	114.9	115.0	115.2	115.3/114.9
M-X [2]	0.451	0.504	0.782	-
A [3]	175.3	174.0	164.6	180

[1] P is the coordination cavity perimeter (in Å). [2] X is dummy atom located in center between N_p atoms. [3] α is the dihedral angle between planes of opposite pyrrole rings.

The degree of the doming-distortion can be described by the distance M-X between the metal atom and the center of the plane formed by four nitrogen atoms N_p and the dihedral angle between the planes of opposite pyrrole rings α. The distance M-X increases in line with the size of a metal atom. Furthermore, the dihedral angle between the opposite pyrrole fragments α decreases by 10 degrees from Ga to In, while a slight change in this parameter is noted from Al to Ga (r_{ionic}(Al) = 0.39, r_{ionic}(Ga) = 0.47, r_{ionic}(In) = 0.62) [28]. Structural parameters of the TPyzPA macrocyclic ligand are practically independent of the nature of a metal atom and peripheral –Cl substitution. The only noticeable change occurs for the peripheral C_γ-C_γ bond that is 0.025 Å longer in the $TPyzPACl_8$ metal complexes due to the electron-withdrawing effect of the –Cl substituents. A similar picture was previously observed for the complexes of tetrabenzoporphyrin with Al(Cl), Ga(Cl), In(Cl) [10] and porphyrazine, and tetrakis(1,2,5-thiadiazole)porphyrazine with Y(Cl), La(Cl) and Lu(Cl) [29]. The perimeter of the coordination cavity is not affected by the nature of a metal atom and increases by ca. 0.05 Å in the metal complexes as compared to the metal-free $H_2TPyzPA$ and $H_2TPyzPACl_8$; nevertheless, the distances between the nitrogen atoms of pyrrole fragments $(N_p \ldots N_p)_{opp}$ and $(N_p \ldots N_p)_{adj}$ are noticeably different (up to 0.2 Å). This can be explained by the fact that in the Al-Ga-In series, there is a consistent decrease in distances N_p-C_α along with valence angles $\angle(MN_pC_\alpha)$ and an increase in C_α-N_m distances and $\angle(C_\alpha N_m C_\alpha)$, which leads to the possibility of a significant difference in distances $(N_p \ldots N_p)_{opp}$ and $(N_p \ldots N_p)_{adj}$ without noticeable perimeter change.

2.2. NBO-Analysis

To gain a deeper insight into the electronic structures of M(Cl)TPyzPA and M(Cl)TPyz $PACl_8$ complexes and features of the metal–ligand chemical bonding, we performed the NBO-analysis of the electron density distribution. The obtained results suggest that the chemical bonding between a metal atom and $TPyzPACl_8$ macrocyclic ligand can be described in terms of the donor–acceptor interactions of the types: LP(N) → ns(M) and LP(N) → np(M), where n is the principal quantum number for the valence shell of the metal atom (n = 3 for Al, n = 4 for Ga, n = 5 for In). It should be noted that in the case of Al complexes, the interactions occur between LP(N) and two 3p(Al) orbitals, while for the complexes of Ga and In, all three valence p-orbitals provide a favorable overlap (Figure 2).

Comparing periphery-substituted $TPyzPACl_8$ complexes with their non-substituted analogues (Table 2), we found that peripheral –Cl substituents do not affect the characteristics of the metal–ligand bonding. The enhanced covalent contribution into the Ga–N bond is in line with the trend of the electronegativities of the metal atoms: Al (χ = 1.47), Ga (χ = 1.82) and In (χ = 1.49) [30,31]. According to Table 2, the NPA charge of Al is the most positive, in contrast to the NPA charge of Ga. More than that, an analogical situation is observed for the negativity of NPA charges of chlorine atoms. Therefore, these charges also correlate with the electronegativities of the metals.

Table 2. Selected parameters of M(Cl)PyzPA complexes from NBO calculations.

	Al(Cl) TPyzPA	**Al(Cl) $TPyzPACl_8$**	**Ga(Cl) TPyzPA**	**Ga(Cl) $TPyzPACl_8$**	**In(Cl) TPyzPA**	**In(Cl) $TPyzPACl_8$**
E(HOMO),eV	−6.329	−6.803	−6.362	−6.836	−6.411	−6.882
E(LUMO),eV	−3.815	−4.294	−3.829	−4.308	−3.864	−4.343
Δ*E*, eV	2.514	2.509	2.533	2.528	2.547	2.539
q(M) NPA, *e*	1.718	1.716	1.637	1.635	1.694	1.692
q(N) NPA, *e*	−0.651	−0.651	−0.631	−0.631	−0.623	−0.623
q(Cl) NPA, *e*	−0.550	−0.545	−0.523	−0.518	−0.528	−0.521
configuration	$3s^{0.42}3p^{0.83}$	$3s^{0.42}3p^{0.83}$	$4s^{0.53}4p^{0.81}$	$4s^{0.53}4p^{0.81}$	$5s^{0.54}5p^{0.76}$	$5s^{0.54}5p^{0.76}$
∑ *E*(d-a), kcal mol^{-1}	526.0	526.5	539.6	539.0	510.7	507.8
Q(M-N), *e*	0.335	0.330	0.343	0.342	0.327	0.325
r(M-N), Å	1.981	1.980	2.022	2.021	2.161	2.162

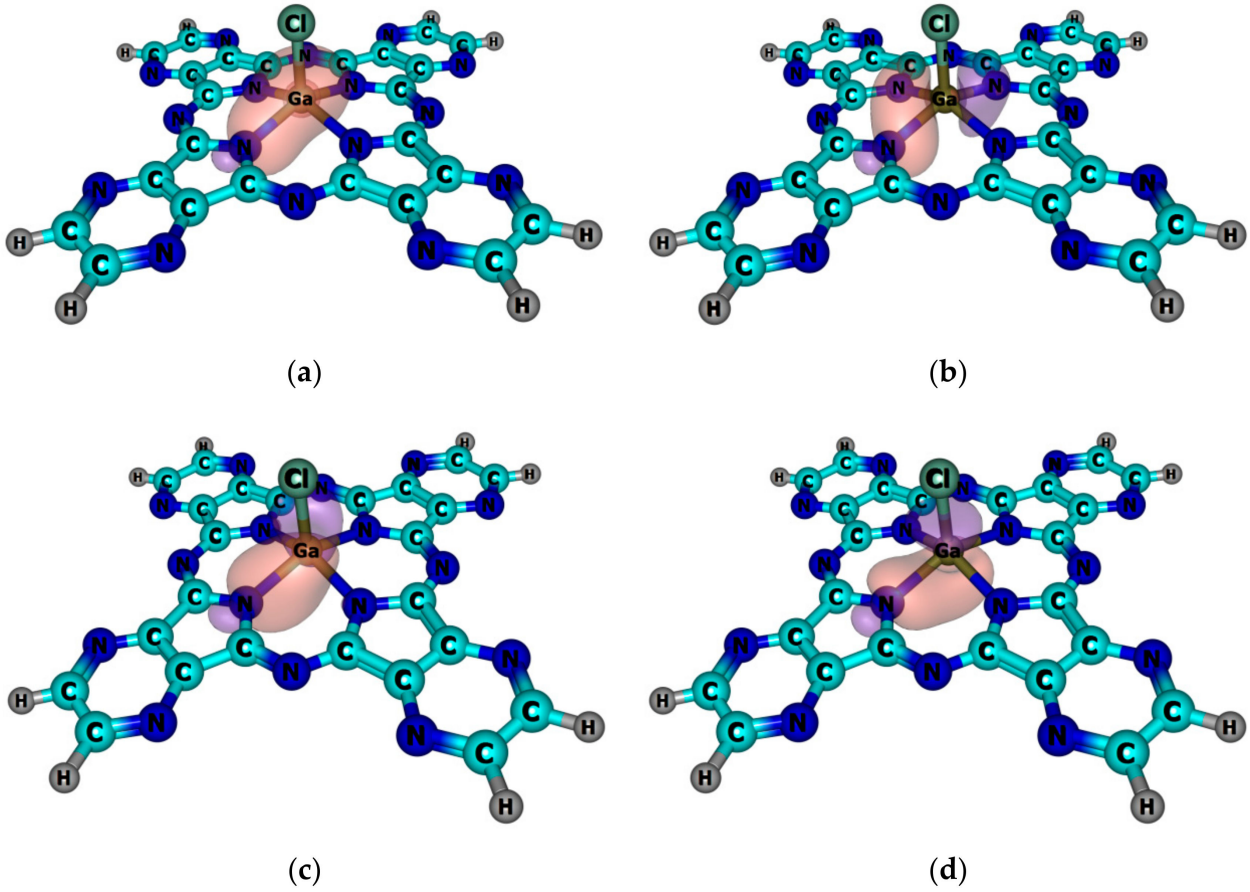

Figure 2. Schemes of the dominant donor–acceptor interactions between Ga and TPyzPA ligand. (**a**) The result of the orbital interaction of the type LP(N) → 4s(Ga) ($E^{(2)}$ = 59.2 kcal mol^{-1}); (**b**) the result of the orbital interaction of the type LP(N) → $4p_x$(Ga) ($E^{(2)}$ = 30.7 kcal mol^{-1}); (**c**) the result of the orbital interaction of the type LP(N) → $4p_y$(Ga) ($E^{(2)}$ = 30.7 kcal mol^{-1}); (**d**) the result of the orbital interaction of the type LP(N) → $4p_z$(Ga) ($E^{(2)}$ = 14.3 kcal mol^{-1}). Only one of the four corresponding interactions is demonstrated.

2.3. Electronic Absorption Spectra

Analyzing the absorption spectra (Figure 3), we can note that three intense absorption bands are observed in the visible light and near UV in the case of M(Cl)TPyzPACl_8, in contrast to M(Cl)TPyzPA, of which spectra contain only two bands in the visible light and near UV range. The B_1-band in the latter has low oscillator strength, so it is practically imperceptible in the absorption spectrum, while this peak is clearly observed in the perchlorinated complexes. This can be related to the fact that the peripheral Cl atoms contribute significantly to $6a_1$ molecular orbital (MO) in M(Cl)TPyzPACl_8 in contrast to the hydrogen atoms in M(Cl)TPyzPA to $3a_1$ MO (Figure S1). The B_1-band is predominantly formed by the electron transitions from these orbitals to doubly-degenerated LUMOs (Table 3).

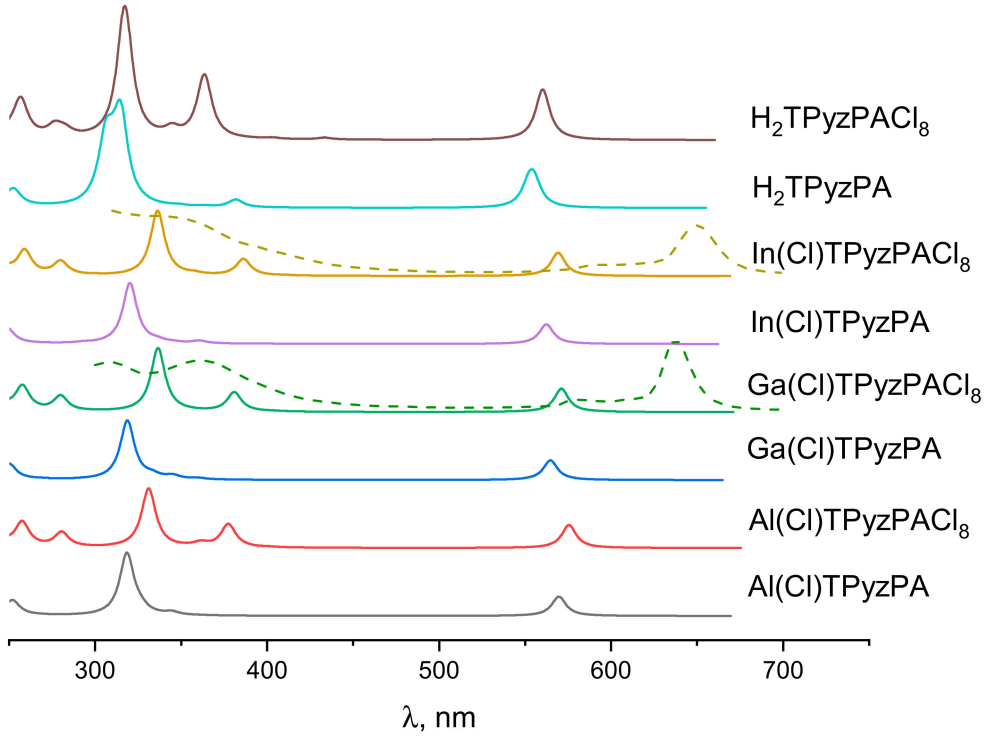

Figure 3. Simulated (solid lines) and experimental (dashed lines) electronic absorption spectra for M(Cl)TpyzPA and M(Cl)TPyzPACl$_8$ (M = Al, Ga, In) and its metal-free complexes.

It can be seen that the position of the Q-band maxima in the electronic absorption spectra shifted bathochromically in the series Ga < Al < In. The changes in the theoretical and experimental spectra are similar to each other and therefore allow the nature of the results obtained to be explained. This indicates that the HOMO–LUMO gap is influenced not only by the degree of doming-distortion of the macrocycle, but also by electronegativity of the central metal, which is the highest for Ga. In addition, a minor bathochromic shift of the Q-band occurs for perchlorinated complexes M(Cl)TPyzPACl$_8$ as compared to M(Cl)TPyzPA. Noteworthy is the single absorption maximum (B-band) in the near UV Soret region (300–420 nm) that appears for M(Cl)TPyzPA, while B_1- and B_2-bands are present for M(Cl)TPyzPACl$_8$. Experimental spectra of Ga(OH)TPyzPACl$_8$ and In(OH)TPyzPACl$_8$ can be found in ESI (Figures S2 and S3).

In addition, attention should be paid to the pronounced hyperchromic effect in metal-free complexes caused by the superposition of several absorption bands with close wavelengths. The composition of the excited states forming the absorption bands is given in Table 3.

It can be seen that the excited states of the compounds under consideration are formed as a result of similar sets of electron transitions. The main composition of the excited states responsible for the Q-band consists of transitions between the frontier π-orbitals. Hence Q-band wavelengths correlate with the HOMO–LUMO gaps. The molecular orbitals level diagram is shown in Figure 4. Stabilization of LUMO upon peripheral chlorination of the TPyzPA macrocycle correlates with the electrochemical data [8], indicating that the reduction potentials for Cl$_8$TPyzPA complexes are shifted by 0.4–0.5 V in a less negative region as compared to the values typical for unsubstituted TPyzPA complexes [10]. It is also worth noting that the 1^1E states are formed mainly by Gouterman-type transitions $a_2 \rightarrow e^*$ for metal complexes and transitions of the $a_u \rightarrow b_{1g}$ and $a_u \rightarrow b_{3g}$ types for metal-free ones due to the lower symmetry of the latter [32–34]. The situation is typical for a number of macrocycles of similar structure [35–37]. Despite the fact that the higher energy states are formed by almost the same electronic transitions, they have a different composition, and therefore energy.

Table 3. Calculated composition of the lowest excited states and corresponding oscillator strengths for TPyzPA and TPyzPzCl_8 complexes.

Al(Cl)TPyzPA					**Al(Cl)TPyzPACl_8**				
State	Composition (%)	λ, nm	*f*	exp. λ, nm	State	Composition (%)	λ, nm	*f*	exp. λ, nm
1^1E	$4a_1 \rightarrow 1e^*$ (8) $3a_2 \rightarrow 1e^*$ (90)	570	0.31		1^1E	$5a_1 \rightarrow 1e^*$ (5) $3a_2 \rightarrow 1e^*$ (90)	576	0.37	643
7^1E	$3a_1 \rightarrow 1e^*$ (54) $2b_2 \rightarrow 1e^*$ (17) $4a_1 \rightarrow 1e^*$ (22)	327	0.07		4^1E	$2b_1 \rightarrow 1e^*$ (5) $6a_1 \rightarrow 1e^*$ (77) $3b_1 \rightarrow 1e^*$ (7) $3a_2 \rightarrow 2e^*$ (5)	377	0.37	
9^1E	$3a_1 \rightarrow 1e^*$ (27) $4a_1 \rightarrow 1e^*$ (58) $3a_2 \rightarrow 1e^*$ (6) $3a_2 \rightarrow 2e^*$ (6)	318	1.00		8^1E	$5a_1 \rightarrow 1e^*$ (70) $6a_1 \rightarrow 1e^*$ (7) $3a_2 \rightarrow 1e^*$ (7) $3a_2 \rightarrow 2e^*$ (9)	331	0.95	363
Ga(Cl)TPyzPA					Ga(Cl)TPyzPACl_8				
State	Composition (%)	λ, nm	*f*	exp. λ, nm	State	Composition (%)	λ, nm	*f*	exp. λ, nm
1^1E	$4a_1 \rightarrow 1e^*$ (8) $3a_2 \rightarrow 1e^*$ (90)	565	0.32		1^1E	$5a_1 \rightarrow 1e^*$ (6) $3a_2 \rightarrow 1e^*$ (90)	571	0.38	638
7^1E	$3a_1 \rightarrow 1e^*$ (26) $2b_2 \rightarrow 1e^*$ (34) $4a_1 \rightarrow 1e^*$ (32)	333	0.05		4^1E	$5a_1 \rightarrow 1e^*$ (6) $6a_1 \rightarrow 1e^*$ (75) $4b_2 \rightarrow 1e^*$ (13)	381	0.31	
9^1E	$3a_1 \rightarrow 1e^*$ (47) $4a_1 \rightarrow 1e^*$ (38) $3a_2 \rightarrow 1e^*$ (6) $3a_2 \rightarrow 2e^*$ (5)	319	0.95		8^1E	$5a_1 \rightarrow 1e^*$ (63) $6a_1 \rightarrow 1e^*$ (8) $3a_2 \rightarrow 1e^*$ (8) $3a_2 \rightarrow 2e^*$ (16)	337	1.03	360
In(Cl)TPyzPA					In(Cl)TPyzPACl_8				
State	Composition (%)	λ, nm	*f*	exp. λ, nm	State	Composition (%)	λ, nm	*f*	exp. λ, nm
1^1E	$4a_1 \rightarrow 1e^*$ (8) $3a_2 \rightarrow 1e^*$ (89)	562	0.32	589	1^1E	$3a_2 \rightarrow 1e^*$ (90) $5a_1 \rightarrow 1e^*$ (6)	569	0.38	649
7^1E	$3a_1 \rightarrow 1e^*$ (36) $2b_2 \rightarrow 1e^*$ (26) $4a_1 \rightarrow 1e^*$ (28) $3a_2 \rightarrow 2e^*$ (7)	336	0.04	335	4^1E	$6a_1 \rightarrow 1e^*$ (76) $5a_1 \rightarrow 1e^*$ (6) $3b_2 \rightarrow 1e^*$ (14)	386	0.26	
9^1E	$3a_1 \rightarrow 1e^*$ (43) $4a_1 \rightarrow 1e^*$ (39) $3a_2 \rightarrow 1e^*$ (7) $3a_2 \rightarrow 2e^*$ (7)	320	0.98		8^1E	$5a_1 \rightarrow 1e^*$ (55) $6a_1 \rightarrow 1e^*$ (6) $3a_2 \rightarrow 1e^*$ (8) $3a_2 \rightarrow 2e^*$ (22)	336	1.05	339
H_2TPyzPA					H_2 TPyzPACl_8				
State	Composition (%)	λ, nm	*f*	exp. λ, nm	State	Composition (%)	λ, nm	*f*	exp. λ, nm
1^1B_{1u}	$3a_u \rightarrow 1b_{1g}^*$ (90) $3a_u \rightarrow 1b_{3g}^*$ (86)	555	0.35	645	1^1B_{1u}	$3a_u \rightarrow 1b_{1g}^*$ (90) $1b_{2u} \rightarrow 1b_{1g}^*$ (5)	560	0.43	656
1^1B_{3u}	$2b_{2u} \rightarrow 1b_{1g}^*$ (5) $3b_{2u} \rightarrow 1b_{1g}^*$ (8)	552	0.33	611	1^1B_{3u}	$2b_{2u} \rightarrow 1b_{1g}^*$ (7) $3a_u \rightarrow 1b_{3g}^*$ (86)	560	0.39	626
2^1B_{3u}	$2b_{2u} \rightarrow 1b_{1g}^*$ (12) $3b_{2u} \rightarrow 1b_{1g}^*$ (80)	382	0.12		3^1B_{3u}	$1b_{2u} \rightarrow 1b_{1g}^*$ (5) $2b_{2u} \rightarrow 1b_{1g}^*$ (85) $3a_u \rightarrow 2b_{3g}^*$ (5)	364	0.78	358
4^1B_{3u}	$1b_{2u} \rightarrow 1b_{1g}^*$ (7) $2b_{2u} \rightarrow 1b_{1g}^*$ (66) $3b_{2u} \rightarrow 1b_{1g}^*$ (9) $3a_u \rightarrow 1b_{3g}^*$ (9) $3a_u \rightarrow 2b_{3g}^*$ (6)	315	1.32	330	4^1B_{1u}	$1b_{2u} \rightarrow 1b_{3g}^*$ (18) $2b_{2u} \rightarrow 1b_{3g}^*$ (78)	362	0.26	358
4^1B_{1u}	$1b_{2u} \rightarrow 1b_{3g}^*$ (62) $2b_{2u} \rightarrow 1b_{3g}^*$ (33) $1b_{2u} \rightarrow 1b_{3g}^*$ (33)	311	0.29		4^1B_{3u}	$1b_{2u} \rightarrow 1b_{1g}^*$ (6) $3a_u \rightarrow 2b_{3g}^*$ (91)	345	0.13	
5^1B_{1u}	$2b_{2u} \rightarrow 1b_{3g}^*$ (42) $3b_{2u} \rightarrow 1b_{3g}^*$ (10) $3a_u \rightarrow 1b_{1g}^*$ (6) $3a_u \rightarrow 2b_{1g}^*$ (5)	306	0.94		5^1B_{3u}	$1b_{2u} \rightarrow 1b_{1g}^*$ (79) $3a_u \rightarrow 1b_{3g}^*$ (8)	319	0.88	
					5^1B_{1u}	$1b_{2u} \rightarrow 1b_{3g}^*$ (68) $2b_{2u} \rightarrow 1b_{3g}^*$ (12)	316	1.34	

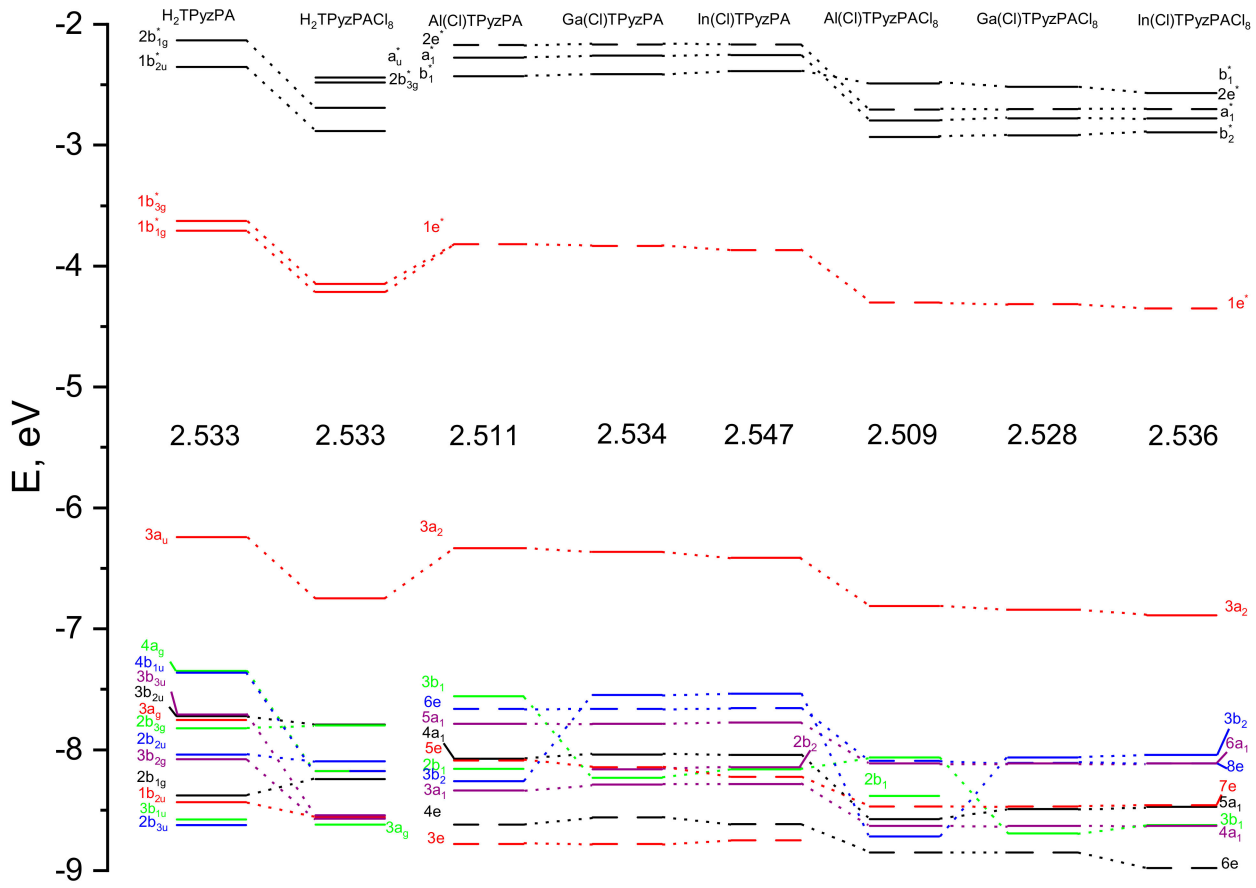

Figure 4. Molecular orbitals (MO) level diagram for H_2TPyzPA, H_2TPyzPACl_8, M(Cl)TPyzPA and M(Cl)TPyzPACl_8 complexes. The values of higher occupied molecular orbital–lowest unoccupied molecular orbital (HOMO–LUMO) gaps are given in eV.

Considering the shapes of the molecular orbitals (MOs) involved in the most probable electronic transitions, we can conclude that the metal nature should not affect the Q-band position since the boundary MOs are the linear combination of atomic orbitals (LCAO) of the macrocyclic ligand. Nevertheless, the size of the coordination cavity depends on the metal nature: changing the geometric structure provides an indirect effect on the position of the Q-band. Moreover, the shape of the LUMOs depends on the metal nature (Figure S1). In the case of Al, it consists of the bonding π-orbitals lying along the C_α-C_β bond and antibonding π-orbitals located around the C_α-N_m and C_α-N_p bonds, while for Ga and In, the C_α-N_p bonds have a significant contribution to the bonding π-orbital, probably due to the influence of the d-sublevel of the metal. The HOMO consists of the AOs localized on carbon atoms of pyrrolic fragments, which is a typical picture for porphyrazines [10,19,25,38]. Note that peripheral Cl atoms contribute to the formation of the MOs involved in the electronic transitions corresponding to the B_1-band in the absorption spectrum. For the rest, the MO's form is similar for all compounds; therefore, it can be concluded that the ligand rather than metal has a decisive influence on the absorption spectrum.

2.4. IR Spectra

The IR spectra were simulated on the basis of the normal mode frequencies and band intensities, which have been calculated by the DFT (PBE0/def2-TZVP) method in a harmonic approximation.

Bands of weak intensity appear in the region up to 600 cm^{-1}, as well as the shift of bands in the range from 600 to 1000 cm^{-1} occurs with the substitution of hydrogen atoms by the metal. It should be noted that the most intensive vibrational transitions

of the metal complexes are degenerate, while the splitting of the bands in the case of the metal-free H_2TPyzPA and H_2TPyzPACl_8 is observed due to the lower symmetry. It results in two peaks with close frequencies formed by the normal vibrations of the pyrrole and pyrrolenine fragments. A medium peak of the N_p-H stretching at 3552 cm^{-1} and 3554 cm^{-1} (H_2TPyzPA and H_2TPyzPACl_8, respectively) is typical for macrocycles such as porphyrazines [25]. According to the experimental data [8,26], these frequencies are 3286 and 3287 cm^{-1}, respectively.

In-plane vibrations contribute to the medium band at 1400 cm^{-1} in the spectra of M(Cl)TPyzPA. Noteworthy are the main differences in the M(Cl)TPyzPA IR spectra observed in the range of 300–600 cm^{-1} related to the weak bands with a strong contribution of the M-Cl stretching.

It is worth noting that a low-frequency band shift occurs in both M(Cl)TPyzPA and M(Cl)TPyzPACl_8 in the Al→Ga→In series. Among the most intense peaks, the only exception is the ω_{92}-ω_{93} band at the ~1140 cm^{-1} for MTPyzPA, which corresponds to in-plane vibrations of the macrocyclic core. Moreover, a significant decrease in these bands' intensity occurs with an increase in the ionic radius of a metal [28].

The IR spectra of M(Cl)TPyzPA are similar in the range of 600–3500 cm^{-1} where the influence of the metal is almost absent. The replacement of H by Cl leads to the vanishing of the bands at 3190 cm^{-1}, corresponding to the C-H stretching vibrations, and an increase in the relative intensity of the peaks in the 800–1300 cm^{-1} region. Simulated spectra are shown in Figure 5. The most intense bands at ~1250 cm^{-1} of all investigated compounds are predominantly stretching vibrations of the bonds of pyrazine rings. Unlike M(Cl)TPyzPA spectra with one peak with a relative intensity >50%, the M(Cl)TPyzPACl_8 spectra also contain the strong bands ω_{117}-ω_{118}, composed by N_d-C_γ and C_β-N_d stretching vibrations. Moreover, M(Cl)TPyzPACl_8 spectra include more relatively intense peaks compared to MTPyzPA. A description of the main vibrations is listed in Table 4 (full list of the most active vibrations can be found in Supplementary Materials, Table S1). It is important to mention that the calculated spectra of Ga(Cl)TPyzPACl_8 and In(Cl)TPyzPACl_8 are consistent with the experimental ones with a factor ~0.95. Actually, the main differences may be caused by another axial ligand (OH instead of Cl). Experimental spectra can be found in ESI (Figures S4 and S5).

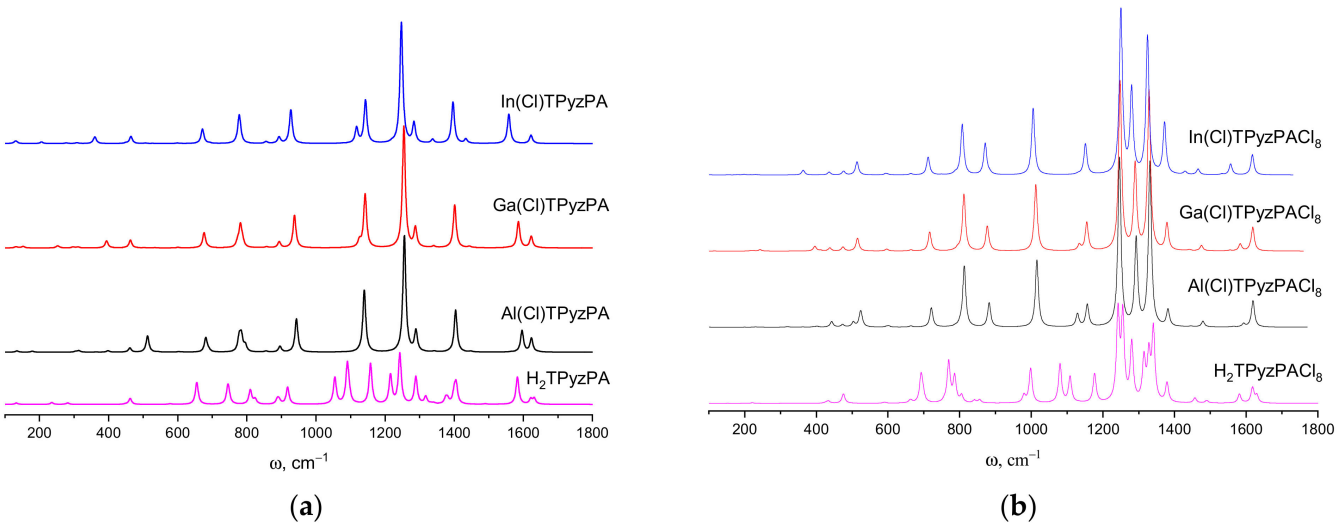

Figure 5. Calculated IR spectra of M(Cl)TPyzPA (**a**) and M(Cl)TPyzPACl_8 (**b**).

Table 4. Assignment of the IR vibrations of the M(Cl)TPyzPA and M(Cl)TPyzPACl_8 complexes.

Frequency, cm^{-1}	I_{rel}, %	Symmetry	Assignment [1]	Exp, cm^{-1}
H_2TPyzPA				KBr [26]
1091 (ω_{86})	78	B_{1u}	r(N_p-C_α) (29), r(N_m-C_α) (18), r(N_d-C_γ) (10), r(C_γ-C_γ) (12)	1040
1157 (ω_{90})	81	B_{2u}	r(N_p-C_α) (23), r(N_m-C_α) (18), r(C_α-C_β) (6), r(C_β-N_d) (8), r(N_d-C_γ) (6), φ(C_α-N_p-H_c) (8), φ(C_β-N_d-C_γ) (7)	1121
1242 (ω_{95})	100	B_{1u}	r(C_α-C_β) (14), r(C_β-C_β) (10), r(N_d-C_γ) (10), φ(N_d-C_γ-H_s) (7)r(C_β-N_d) (6), r(C_β-C_β) (42), r(C_γ-Cl) (26), φ(N_d-C_γ-Cl) (6)	1198
3193 (ω_{141})	24	B_{2u}	r(H_s-C_γ) (99)	3051
3552 (ω_{143})	45	B_{1u}	r(H_c-N_p) (99)	3286
H_2TPyzPACl_8				KBr [8]
1242 (ω_{107})	100	B_{1u}	r(C_β-N_d) (6), r(C_β-C_β) (42), r(C_γ-Cl) (26), φ(N_d-C_γ-Cl) (6)	1192
1255 (ω_{109})	98	B_{2u}	r(C_β-N_d) (8), r(C_γ-C_γ) (46), r(C_γ-Cl) (21), φ(N_d-C_γ-Cl) (6)	1235
1281 (ω_{111})	67	B_{1u}	r(C_α-C_β) (8), r(C_β-C_β) (19), r(N_d-C_γ) (13), r(C_γ-C_γ) (13)	
1328 (ω_{116})	52	B_{1u}	r(N_p-C_α) (7), r(N_m-C_α) (11), r(C_β-N_d) (12), r(N_d-C_γ) (45)	
1340 (ω_{117})	83	B_{2u}	r(N_p-C_α) (8), r(C_α-C_β) (10), r(C_β-C_β) (8), r(C_β-N_d) (19), φ(C_α-N_p-H_c) (28)	
3554 (ω_{143})	27	B_{1u}	r(H_c-N_p) (99)	3287

Table 4. *Cont.*

Frequency, cm^{-1}	I_{rel}, %	Symmetry	Assignment [1]	Exp, cm^{-1}
Al(Cl)TPyzPA				
1140 (ω_{92}-ω_{93})	53	E	r(N_p-C_α) (24), r(N_m-C_α) (14), r(C_α-C_β) (10), r(C_β-N_d) (12), r(N_d-C_γ) (9)	
1255 (ω_{98}-ω_{99})	100	E	r(N_p-C_α) (5), r(C_α-C_β) (15), r(C_β-C_β) (14), r(N_d-C_γ) (20), φ(C_β-N_d-C_γ) (9)	
1404(ω_{113}-ω_{114})	36	E	r(C_β-C_β) (12), r(C_γ-C_γ) (13), φ(N_d-C_γ-H_s) (36), φ(C_γ-C_γ-H_s) (23)	
3189 (ω_{142}-ω_{143})	18	E	r(H_s-N_p) (99)	
Al(Cl)TPyzPACl_8				KBr [8]
1246 (ω_{111}-ω_{112})	100	E	r(C_γ-C_γ) (43), r(C_γ-Cl) (25), φ(N_d-C_γ-Cl) (6)	1168
1293 (ω_{115}-ω_{116})	52	E	r(N_p-C_α) (8), r(C_β-C_β) (15), r(N_d-C_γ) (25), r(C_γ-C_γ) (13)	1260
1331 (ω_{117}-ω_{118})	97	E	r(C_α-C_β) (8), r(C_β-N_d) (23), r(N_d-C_γ) (49)	1323
Ga(Cl)TPyzPA				
1142 (ω_{92}-ω_{93})	44	E	r(N_p-C_α) (49), r(N_m-C_α) (11), r(C_α-C_β) (9), r(N_d-C_γ) (9)	
1254 (ω_{98}-ω_{99})	100	E	r(N_p-C_α) (6), r(C_α-C_β) (12), r(C_β-C_β) (11), r(C_β-N_d) (9), r(N_d-C_γ) (18)	
1401 (ω_{113}-ω_{114})	35	E	r(C_β-C_β) (11), r(C_γ-C_γ) (12), φ(N_d-C_γ-H_s) (36), φ(C_γ-C_γ-H_s) (23)	
3194 (ω_{142}-ω_{143})	17	E	r(H_s-N_p) (99)	
Ga(Cl)TPyzPACl_8				this work
1248 (ω_{111}-ω_{112})	100	E	r(C_γ-C_γ) (41), r(C_γ-Cl) (24), φ(N_d-C_γ-Cl) (6)	1232
1290 (ω_{115}-ω_{116})	50	E	r(N_p-C_α) (6), r(C_α-C_β) (7), r(C_β-C_β) (17), r(N_d-C_γ) (26), r(C_γ-C_γ) (13)	
1328 (ω_{117}-ω_{118})	94	E	r(C_α-C_β) (8), r(C_β-N_d) (22), r(N_d-C_γ) (50)	1349

Table 4. *Cont.*

Frequency, cm^{-1}	I_{rel}, %	Symmetry	Assignment [1]	Exp, cm^{-1}
In(Cl)TPyzPA				KBr [39]
1143 (ω_{92}-ω_{93})	36	E	r(N_p-C_α) (49), r(N_m-C_α) (10), r(C_α-C_β) (6), r(N_d-C_γ) (10)	1100
1247 (ω_{98}-ω_{99})	100	E	r(N_p-C_α) (5), r(C_α-C_β) (15), r(C_β-C_β) (14), r(N_d-C_γ) (20)	1213
1396 (ω_{113}-ω_{114})	34	E	r(C_β-C_β) (10), r(C_γ-C_γ) (10), φ(N_d-C_γ-H_s) (34), φ(C_γ-C_γ-H_s) (22)	1364
3194 (ω_{142}-ω_{143})	17	E	r(H_s-N_p) (99)	3316
In(Cl)TPyzPACl_8				this work
1250 (ω_{111}-ω_{112})	100	E	r(C_γ-C_γ) (44), r(C_γ-Cl) (26), φ(N_d-C_γ-Cl) (6)	1264
1280 (ω_{114}-ω_{115})	50	E	r(N_p-C_α) (5), r(C_α-C_β) (7), r(C_β-C_β) (19), r(N_d-C_γ) (26)	1323
1325 (ω_{117}-ω_{118})	83	E	r(C_α-C_β) (8), r(C_β-N_d) (23), r(N_d-C_γ) (49)	1364

[1] Coordinates are listed provided that their contributions (shown in parentheses) are greater than ~5%. Assignment of vibrational modes based on potential energy distribution. The following designations of the coordinates are used: r—stretching of the bond; φ—bending, a change in the angle; OPB—out-of-plane bending; θ—a change in the dihedral angle. Experimental frequencies are given for metal complexes with an axial–OH ligand.

3. Materials and Methods

3.1. Synthesis

Octachlorotetrapyrazinoporphyrazinatogallium(III) hydroxide, [Ga(OH)TPyzPACl_8]. A mixture of 5,6-dichloropyrazine-2,3-dicarbonitrile (200 mg, 1 mmol) and gallium(III) hydroxydiacetate (50 mg, 0.24 mmol) was melted at 200 °C for 10 min. The obtained solid was powdered, washed with CH_2Cl_2, then dissolved in conc. H_2SO_4, precipitated by pouring into ice-water, centrifuged and washed with MeOH. After drying, the complex was obtained as dark green hydrated material.

Octachlorotetrapyrazinoporphyrazinatoindium(III) hydroxide, [In(OH)TPyzPACl_8]. A mixture of 5,6-dichloropyrazine-2,3-dicarbonitrile (1) (200 mg, 1 mmol) and indium(III) hydroxydiacetate (50 mg, 0.2 mmol) was melted at 200 °C for 10 min. The obtained solid was powdered, washed with CH_2Cl_2, then dissolved in THF and chromatographed on silica with THF as eluent. The eluted product was precipitated by pouring into water, centrifuged and washed with MeOH. After drying, the complex was obtained as dark green hydrated material [8].

The IR spectra were measured on an IR-spectrometer Cary 630 FT-IR using KBr pellets. UV–Vis spectra were recorded using a Cary UV-Vis spectrophotometer in THF solution and can be found in ESI.

3.2. Computational Details

The DFT study of M(Cl)TPyzPA and M(Cl)TPyzPACl_8 included geometry optimization and calculations of the harmonic vibrations, followed by calculation of the electronic absorption spectrum by the TDDFT method. The number of the calculated excited states was 30. The calculations were performed using the PBE0 functional with the density

functional dispersion correction D3 provided by Grimme [40] with the def2-TZVP basis set [41] taken from the EMSL BSE library [42–44]. Firefly QC package [45], which is partially based on the GAMESS (US) [46] source code, was used to obtain the optimized geometry, electronic absorption spectra and NBO-analysis. The optimized Cartesian coordinates of H_2TPyzPA, H_2TPyzPACl_8 and their metal complexes with Al, Ga, In are available in the Supplementary Materials.

The calculations of IR spectra were carried out with use of Gaussian09 [47] software package due to the fact it applies analytical functions in the second derivatives computing. The molecular models and orbitals demonstrated in the paper were visualized by means of the Chemcraft program [48].

4. Conclusions

The geometry and electronic structure of TPyzPA were investigated using PBE0-D3 functional with basis set def2-TZVP. The distance M-X between the metal atom and the center of the plane formed by four nitrogen atoms N_p increases in line with the size of a metal atom. Structural parameters of the TPyzPA macrocyclic ligand are practically independent of the nature of a metal atom and peripheral −Cl substitution. The fact that $(N_p \ldots N_p)_{opp}$ and $(N_p \ldots N_p)_{adj}$ are substantially different for Al, Ga and In complexes, while the perimeter of the coordination cavity almost remains invariant for both M(Cl)TPyzPA and M(Cl)TPyzPACl_8 complexes, indicates that the degree of distortion increases from Al to In. At the same time, the substitution of H-atoms for Cl mainly affects the internuclear distances of pyrazine rings and has a negligible effect on the N_p-C_α and C_α-N_m.

According to the NBO-analysis of electron density distribution, the strong donor–acceptor interactions of the types: LP(N) → ns(M) and LP(N) → np(M), where n is the principal quantum number for the valence shell of the metal atom, stabilize the complexes.

It was found that the HOMO–LUMO gap is slightly affected by the nature of the metal and increases in the Al-Ga-In series. The substitution of H-atoms for Cl leads to a decrease in the energy of the frontier MOs of M(Cl)TPyzPACl_8 as compared to M(Cl)TPyzPA. Furthermore, the LUMO is stabilized much more than the HOMO, resulting in a smaller HOMO–LUMO gap.

Simulated electronic absorption spectra show that the metal nature slightly influences the position of the band's position. In the series Al→Ga→In→H_2, the Q-band is shifted to a shorter wavelength. In addition, a minor bathochromic shift occurs in M(Cl)TPyzPA compared to M(Cl)TPyzPACl_8. The excited states corresponding to the Q-bands are composed mainly of Gouterman-type transitions. The electronic absorption spectra of TPyzPACl_8 contain three intense maxima, while only two peaks were found for TPyzPA. The additional B_1 band in the M(Cl)TPyzPACl_8 spectra is caused by the transitions from MOs with a contribution of AOs of the peripheral Cl atoms.

The calculated IR spectra of TPyzPACl_8 have a significant difference in comparison with TPyzPA due to heavy Cl atoms being involved in the vibrations that form medium and strong bands in the region of 1000–1500 cm^{-1}.

Supplementary Materials: The following supporting information can be downloaded at: https://www.mdpi.com/article/10.3390/ijms23105379/s1.

Author Contributions: Conceptualization, P.A.S. and Y.A.Z.; methodology, P.A.S. and Y.A.Z.; investigation, I.V.R., A.V.E. and D.N.F.; resources, Y.A.Z.; data curation, A.V.E. and I.V.R.; writing—original draft preparation, A.V.E. and I.V.R. All authors have read and agreed to the published version of the manuscript.

Funding: This work is supported by the Russian Science Foundation (grant No. 21-73-10126).

Institutional Review Board Statement: Not applicable.

Informed Consent Statement: Not applicable.

Data Availability Statement: The data presented in this study are available on request from the corresponding author.

Acknowledgments: The research was carried out using the resources of the Center for Shared Use of Scientific Equipment of the ISUCT (with the support of the Ministry of Science and Higher Education of Russia, grant No. 075-15-2021-671). The authors are grateful to Arseniy A. Otlyotov for helpful suggestions and discussions.

Conflicts of Interest: The authors declare no conflict of interest.

References

1. De la Torre, G.; Vázquez, P.; Agulló-López, F.; Torres, T. Role of structural factors in the nonlinear optical properties of phthalocyanines and related compounds. *Chem. Rev.* **2004**, *104*, 3723–3750. [CrossRef] [PubMed]
2. Drobizhev, M.; Makarov, N.S.; Rebane, A.; De La Torre, G.; Torres, T. Strong two-photon absorption in Push-Pull phthalocyanines: Role of resonance enhancement and permanent dipole moment change upon excitation. *J. Phys. Chem. C* **2008**, *112*, 848–859. [CrossRef]
3. Senge, M.O.; Fazekas, M.; Notaras, E.G.A.; Blau, W.J.; Zawadzka, M.; Locos, O.B.; Mhuircheartaigh, E.M.N. Nonlinear optical properties of porphyrins. *Adv. Mater.* **2007**, *19*, 2737–2774. [CrossRef]
4. McEwan, K.; Lewis, K.; Yang, G.Y.; Chng, L.L.; Lee, Y.W.; Lau, W.P.; Lai, K.S. Synthesis, Characterization, and Nonlinear Optical Study of Metalloporphyrins. *Adv. Funct. Mater.* **2003**, *13*, 863–867. [CrossRef]
5. Marder, S.R. Organic nonlinear optical materials: Where we have been and where we are going. *Chem. Commun.* **2006**, *2*, 131–134. [CrossRef]
6. Liu, F.; Qin, G.; Li, Z.; Wang, Z.; Peng, M.; Wu, S.; Li, C.; Yang, Y. The design and synthesis of nonlinear optical chromophores containing two short chromophores for an enhanced electro-optic activity†. *Mater. Adv.* **2021**, *2*, 728. [CrossRef]
7. Koifman, O.I.; Ageeva, T.A.; Beletskaya, I.P.; Averin, A.D.; Yakushev, A.A.; Tomilova, L.G.; Dubinina, T.V.; Tsivadze, A.Y.; Gorbunova, Y.G.; Martynov, A.G.; et al. Macroheterocyclic compounds—A key building block in new functional materials and molecular devices. *Macroheterocycles* **2020**, *13*, 311–467. [CrossRef]
8. Hamdoush, M.; Ivanova, S.S.; Koifman, O.I.; Kos'kina, M.; Pakhomov, G.L.; Stuzhin, P.A. Synthesis, spectral and electrochemical study of perchlorinated tetrapyrazinoporphyrazine and its AlIII, GaIII and InIII complexes. *Inorg. Chim. Acta* **2016**, *444*, 81–86. [CrossRef]
9. Kosov, A.D.; Dubinina, T.V.; Borisova, N.E.; Ivanov, A.V.; Drozdov, K.A.; Trashin, S.A.; De Wael, K.; Kotova, M.S.; Tomilova, L.G. Novel phenyl-substituted pyrazinoporphyrazine complexes of rare-earth elements: Optimized synthetic protocols and physicochemical properties. *New J. Chem.* **2019**, *43*, 3153–3161. [CrossRef]
10. Novakova, V.; Donzello, M.P.; Ercolani, C.; Zimcik, P.; Stuzhin, P.A. Tetrapyrazinoporphyrazines and their metal derivatives. Part II: Electronic structure, electrochemical, spectral, photophysical and other application related properties. *Coord. Chem. Rev.* **2018**, *361*, 1–73. [CrossRef]
11. Konovalov, A.I.; Antipin, I.S.; Burilov, V.A.; Madzhidov, T.I.; Kurbangalieva, A.R.; Nemtarev, A.V.; Solovieva, S.E.; Stoikov, I.I.; Mamedov, V.A.; Zakharova, L.Y.; et al. Modern Trends of Organic Chemistry in Russian Universities. *Russ. J. Org. Chem.* **2018**, *54*, 157–371. [CrossRef]
12. Skvortsov, I.A.; Kovkova, U.P.; Zhabanov, Y.A.; Khodov, I.A.; Somov, N.V.; Pakhomov, G.L.; Stuzhin, P.A. Subphthalocyanine-type dye with enhanced electron affinity: Effect of combined azasubstitution and peripheral chlorination. *Dyes Pigments* **2021**, *185*, 108944. [CrossRef]
13. Donzello, M.P.; Ercolani, C.; Novakova, V.; Zimcik, P.; Stuzhin, P.A. Tetrapyrazinoporphyrazines and their metal derivatives. Part I: Synthesis and basic structural information. *Coord. Chem. Rev.* **2016**, *309*, 107–179. [CrossRef]
14. Ustimenko, K.A.; Konarev, D.V.; Khasanov, S.S.; Lyubovskaya, R.N. Synthesis of iron(II) octachlorotetrapyrazinoporphyrazine, molecular structure and optical properties of the (X-)2FeTPyzPACl8 dianions with two axial anionic ligands (X- = CN-, CL-). *Macroheterocycles* **2013**, *6*, 345–352. [CrossRef]
15. Faraonov, M.A.; Romanenko, N.R.; Kuzmin, A.V.; Konarev, D.V.; Khasanov, S.S.; Lyubovskaya, R.N. Crystalline salts of the ring-reduced tin(IV) dichloride hexadecachlorophthalocyanine and octachloro- and octacyanotetrapyrazinoporphyrazine macrocycles with strong electron-withdrawing ability. *Dyes Pigments* **2020**, *180*, 108429. [CrossRef]
16. Eroshin, A.V.; Otlyotov, A.A.; Kuzmin, I.A.; Stuzhin, P.A.; Zhabanov, Y.A. DFT Study of the Molecular and Electronic Structure of Metal-Free Tetrabenzoporphyrin and Its Metal Complexes with Zn, Cd, Al, Ga, In. *Int. J. Mol. Sci.* **2022**, *23*, 939. [CrossRef]
17. Hohenberg, P.; Kohn, W. Inhomogeneous electron gas. *Phys. Rev.* **1964**, *136*, B864. [CrossRef]
18. Kohn, W.; Sham, L.J. Self-consistent equations including exchange and correlation effects. *Phys. Rev.* **1965**, *140*, A1133–A1138. [CrossRef]
19. Zhabanov, Y.A.; Tverdova, N.V.; Giricheva, N.I.; Girichev, G.V.; Stuzhin, P.A. DFT Study of molecular and electronic structure of magnesium (II) tetra(1,2,5-chalcogenadiazolo) porphyrazines, [TXDPzMg] (X = O, S, Se, Te). *J. Porphyr. Phthalocyanines* **2017**, *21*, 439–452. [CrossRef]
20. Yablokova, L.I.A.; Ivanova, S.S.; Novakova, V.; Zhabanov, Y.A.; Stuzhin, P.A. Perfluorinated porphyrazines. 3. Synthesis, spectral-luminescence and electrochemical properties of perfluorinated octaphenylporphyrazinatozinc(II). *J. Fluor. Chem.* **2018**, *214*, 86–93.

21. Stuzhin, P.A.; Skvortsov, I.A.; Zhabanov, Y.A.; Somov, N.V.; Razgonyaev, O.V.; Nikitin, I.A.; Koifman, O.I. Subphthalocyanine azaanalogues—Boron(III) subporphyrazines with fused pyrazine fragments. *Dyes Pigments* **2019**, *162*, 888–897. [CrossRef]
22. Otlyotov, A.A.; Zhabanov, Y.A.; Pogonin, A.E.; Kuznetsova, A.S.; Islyaikin, M.K.; Girichev, G.V. Gas-phase structures of hemiporphyrazine and dicarbahemiporphyrazine: Key role of interactions inside coordination cavity. *J. Mol. Struct.* **2019**, *1184*, 576–582. [CrossRef]
23. Hamdoush, M.; Nikitin, K.; Skvortsov, I.; Somov, N.; Zhabanov, Y.; Stuzhin, P.A. Influence of heteroatom substitution in benzene rings on structural features and spectral properties of subphthalocyanine dyes. *Dyes Pigments* **2019**, *170*, 107584. [CrossRef]
24. Eroshin, A.V.; Otlyotov, A.A.; Zhabanov, Y.A.; Veretennikov, V.V.; Islyaikin, M.K. Complexes of Ca(II), Ni(II) and Zn(II) with hemi- and dicarbahemiporphyrazines: Molecular structure and features of metal-ligand bonding. *Macroheterocycles* **2021**, *14*, 119–129. [CrossRef]
25. Zhabanov, Y.A.; Eroshin, A.V.; Stuzhin, P.A.; Ryzhov, I.V.; Kuzmin, I.A.; Finogenov, D.N. Molecular structure, thermodynamic and spectral characteristics of metal-free and nickel complex of tetrakis(1,2,5-thiadiazolo)porphyrazine. *Molecules* **2021**, *26*, 2945. [CrossRef]
26. Konarev, D.V.; Faraonov, M.A.; Kuzmin, A.V.; Osipov, N.G.; Khasanov, S.S.; Otsuka, A.; Yamochi, H.; Kitagawa, H.; Lyubovskaya, R.N. Molecular structures, and optical and magnetic properties of free-base tetrapyrazinoporphyrazine in various reduction states. *New J. Chem.* **2019**, *43*, 19214–19222. [CrossRef]
27. Liu, Z.; Zhang, X.; Zhang, Y.; Jiang, J. The molecular, electronic structures and IR and Raman spectra of metal-free, N,N′-dideuterio, and magnesium tetra-2,3-pyrazino-porphyrazines: Density functional calculations. *Vib. Spectrosc.* **2007**, *43*, 447–459. [CrossRef]
28. Shannon, R.D. Revised effective ionic radii and systematic studies of interatomic distances in halides and chalcogenides. *Acta Crystallogr. Sect. A* **1976**, *32*, 751–767. [CrossRef]
29. Zhabanov, Y.A.; Ryzhov, I.V.; Kuzmin, I.A.; Eroshin, A.V.; Stuzhin, P.A. DFT Study of Molecular and Electronic Structure of Y, La and Lu Complexes with Porphyrazine and Tetrakis(1,2,5-thiadiazole)porphyrazine. *Molecules* **2020**, *26*, 113. [CrossRef]
30. Allred, A.L.; Rochow, E.G. A scale of electronegativity based on electrostatic force. *J. Inorg. Nucl. Chem.* **1958**, *5*, 264–268. [CrossRef]
31. Mann, J.B.; Meek, T.L.; Allen, L.C. Configuration energies of the main group elements. *J. Am. Chem. Soc.* **2000**, *122*, 2780–2783. [CrossRef]
32. Gouterman, M. Spectra of porphyrins. *J. Mol. Spectrosc.* **1961**, *6*, 138–163. [CrossRef]
33. Gouterman, M.; Wagnière, G.H.; Snyder, L.C. Spectra of porphyrins. Part II. Four orbital model. *J. Mol. Spectrosc.* **1963**, *11*, 108–127. [CrossRef]
34. Weiss, C.; Kobayashi, H.; Gouterman, M. Spectra of porphyrins. Part III. Self-consistent molecular orbital calculations of porphyrin and related ring systems. *J. Mol. Spectrosc.* **1965**, *16*, 415–450. [CrossRef]
35. Nemykin, V.N.; Hadt, R.G.; Belosludov, R.V.; Mizuseki, H.; Kawazoe, Y. Influence of molecular geometry, exchange-correlation functional, and solvent effects in the modeling of vertical excitation energies in phthalocyanines using time-dependent density functional theory (TDDFT) and polarized continuum model TDDFT methods: Ca. *J. Phys. Chem. A* **2007**, *111*, 12901–12913. [CrossRef]
36. Belosludov, V.R.; Nevonen, D.; Rhoda, M.H.; Sabin, R.J.; Nemykin, N.V. Simultaneous Prediction of the Energies of Qx and Qy Bands and Intramolecular Charge-Transfer Transitions in Benzoannulated and Non-Peripherally Substituted Metal-Free Phthalocyanines and Their Analogues: No Standard TDDFT Silver Bullet Yet. *J. Phys. Chem. A* **2018**, *123*, 132–152. [CrossRef]
37. Stillman, M.; Mack, J.; Kobayashi, N. Theoretical aspects of the spectroscopy of porphyrins and phthalocyanines. *J. Porphyr. Phthalocyanines* **2002**, *6*, 296–300. [CrossRef]
38. Otlyotov, A.A.; Ryzhov, I.V.; Kuzmin, I.A.; Zhabanov, Y.A.; Mikhailov, M.S.; Stuzhin, P.A. DFT Study of Molecular and Electronic Structure of Ca(II) and Zn(II) Complexes with Porphyrazine and tetrakis(1,2,5-thiadiazole)porphyrazine. *Int. J. Mol. Sci.* **2020**, *21*, 2923. [CrossRef]
39. Dini, D.; Hanack, M.; Meneghetti, M. Nonlinear optical properties of tetrapyrazinoporphyrazinato indium chloride complexes due to excited-state absorption processes. *J. Phys. Chem. B* **2005**, *109*, 12691–12696. [CrossRef]
40. Grimme, S.; Antony, J.; Ehrlich, S.; Krieg, H. A consistent and accurate ab initio parametrization of density functional dispersion correction (DFT-D) for the 94 elements H-Pu. *J. Chem. Phys.* **2010**, *132*, 154104. [CrossRef]
41. Weigend, F.; Ahlrichs, R. Balanced basis sets of split valence, triple zeta valence and quadruple zeta valence quality for H to Rn: Design and assessment of accuracy. *Phys. Chem. Chem. Phys.* **2005**, *7*, 3297–3305. [CrossRef] [PubMed]
42. Schuchardt, K.L.; Didier, B.T.; Elsethagen, T.; Sun, L.; Gurumoorthi, V.; Chase, J.; Li, J.; Windus, T.L. Basis set exchange: A community database for computational sciences. *J. Chem. Inf. Model.* **2007**, *47*, 1045–1052. [CrossRef]
43. Feller, D. The role of databases in support of computational chemistry calculations. *J. Comput. Chem.* **1996**, *17*, 1571–1586. [CrossRef]
44. Pritchard, B.P.; Altarawy, D.; Didier, B.; Gibson, T.D.; Windus, T.L. New Basis Set Exchange: An Open, Up-to-Date Resource for the Molecular Sciences Community. *J. Chem. Inf. Model.* **2019**, *59*, 4814–4820. [CrossRef] [PubMed]
45. Granovsky, A.A. Firefly Version 8. Available online: http://classic.chem.msu.su/gran/firefly/index.html (accessed on 15 April 2021).
46. Schmidt, M.W.; Baldridge, K.K.; Boatz, J.A.; Elbert, S.T.; Gordon, M.S.; Jensen, J.H.; Koseki, S.; Matsunaga, N.; Nguyen, K.A.; Su, S.; et al. General atomic and molecular electronic structure system. *J. Comput. Chem.* **1993**, *14*, 1347–1363. [CrossRef]

47. Frisch, M.J.; Trucks, G.W.; Schlegel, H.B.; Scuseria, G.E.; Robb, M.A.; Cheeseman, J.R.; Scalmani, G.; Barone, V.; Mennucci, B.; Petersson, G.A.; et al. *Gaussian 09*; Revision A.1; Gaussian Inc.: Wallingford, UK, 2009.
48. Zhurko, G.A.; Zhurko, D.A. ChemCraft, Version 1.6 (Build 312); Ed. Available online: http://www.chemcraftprog.com/index.html (accessed on 1 December 2021).